

Mirrored Autoencoders with Simplex Interpolation for Unsupervised Anomaly Detection

Yexin Wu¹, Yogesh Balaji¹, Bhanukiran Vinzamuri², and Soheil Feizi¹

¹ University of Maryland, College Park

² IBM Research

ywu12319@terpmail.umd.edu {yogesh,sfeizi}@cs.umd.edu
bhanu.vinzamuri@ibm.com

Abstract. Use of deep generative models for unsupervised anomaly detection has shown great promise partially owing to their ability to learn proper representations of complex input data distributions. Current methods, however, lack a strong latent representation of the data, thereby resulting in sub-optimal unsupervised anomaly detection results. In this work, we propose a novel representation learning technique using deep autoencoders to tackle the problem of unsupervised anomaly detection. Our approach replaces the L_p reconstruction loss in the autoencoder optimization objective with a novel adversarial loss to enforce semantic-level reconstruction. In addition, we propose a novel simplex interpolation loss to improve the structure of the latent space representation in the autoencoder. Our technique improves the state-of-the-art unsupervised anomaly detection performance by a large margin on several image datasets including MNIST, fashion MNIST, CIFAR and Coil-100 as well as on several non-image datasets including KDD99, Arrhythmia and Thyroid. For example, On the CIFAR-10 dataset, using a standard leave-one-out evaluation protocol, our method achieves a substantial performance gain of 0.23 AUC points compared to the state-of-the-art.

Keywords: Unsupervised anomaly detection, representation learning, generative models.

1 Introduction

Data distributions encountered in different applications are typically noisy and may contain out-of-distribution samples, also called outliers or anomalies [7]. Detecting these anomalous patterns is crucial in many applications: In medical imaging, detecting anomalous patterns in X-ray and MRI scans could aid doctors diagnose patients more effectively [19]. Detecting anomalous behaviour in credit card usage patterns help banks identify fraudulent users [18]. Detecting anomalous objects such as guns in baggage scans can identify hazardous materials in airport screening systems [1]. Anomaly detection systems are also used as a pre-processing step in many machine learning pipelines [9]. For instance,

a system for detecting cats vs. dogs could assign high probability scores to car samples, as it is required to predict car samples as one of the two classes. An anomaly detection step can weed out such anomalous patterns before passing it to the recognition system.

Anomaly detection is a long standing problem in machine learning and computer vision [7, 33]. The problem is typically addressed in a supervised, semi-supervised or unsupervised framework. In supervised and semi-supervised anomaly detection, access to a few (or many) labeled anomalous samples are assumed, and is typically solved as a supervised learning problem. Unsupervised anomaly detection, on the other hand, is a much harder problem than the previous ones as anomalous samples are not available in the training time. Instead, we are given an input dataset, with a goal of detecting any out-of-distribution sample that does not belong to the provided input dataset. The absence of out-of-distribution samples during training makes the unsupervised anomaly detection problem a challenging one.

Unsupervised setting in anomaly detection is an important one to address primarily for the following reasons: In many applications like detecting fraudulent credit card users, number of labeled anomalous samples can be much smaller than normal samples. Supervised classification in this case typically leads to overfitting. Or in some applications, annotating data can be expensive e.g., medical imaging. Even in cases where a few types of anomalous samples are labeled (eg., broken arms in X-ray images), supervised models could achieve high performance in detecting the same type of anomaly. But if a new type of anomaly is presented at test-time, these models fail to generalize. By addressing anomaly detection in unsupervised regime, we focus on detection any class of out-of-distribution samples. Additionally, we do not rely on any labeled information, hence data scarcity is no longer an issue.

Use of deep generative models has received much attention recently for unsupervised anomaly detection. The core idea is to learn the input distribution using a generative model such as a GAN or an auto-encoder, and to flag a sample as anomalous if it lies far away from the generative manifold. Since estimating the distance of a sample from a generative manifold is a hard problem, proxy measures are typically used as anomaly scores. In [23], a linear combination of L_2 distance between images and discriminator feature representations is used as anomaly score. In [1] and [2], an encoder network is learnt with an auto-encoding objective, and the L_2 distance between encoded feature representations of the input and reconstructed image is used as anomaly score. In [4], distance of a test sample from a GAN manifold along with the latent likelihood and an entropy term is proven to be a estimator of sample likelihood, which is a natural candidate for anomaly score.

In this work, we propose a novel approach for unsupervised anomaly detection problem by learning a powerful autoencoder model that contains two novel components. First, we introduce *Mirrored Adversarial Autoencoder*, a variant of autoencoder in which we replace the L_2 loss with an adversarial loss on the joint distribution of input and its mirrored reconstructed samples. As shown in Fig

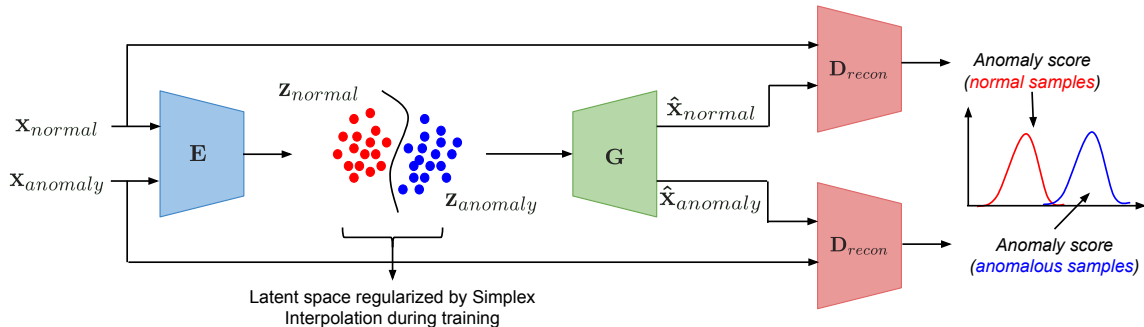


Fig. 1: Anomaly detection pipeline: Given two samples \mathbf{x}_{normal} and $\mathbf{x}_{anomaly}$, we first compute their latent codes using Mirrored Autoencoder (Fig. 3 (b)) trained with Simplex interpolation (Fig. 3 (a)). These latent codes are decoded back to the image space to obtain $\hat{\mathbf{x}}_{normal}$ and $\hat{\mathbf{x}}_{anomaly}$. A discriminator network (used in mirrored auto-encoder training) then extracts the features representations of (input, reconstruction) pairs. These features are used to compute anomaly scores. Use of simplex interpolation and mirrored autoencoders during training gives good latent representations well suited for anomaly detection.

3, the autoencoder model employs a discriminator network that discriminates between (input, input) and (input, reconstruction) pairs, while the encoder-generator pair is trained using an adversarial loss derived from the discriminator network. Second, we extend the interpolation idea proposed in [6] and introduce a novel interpolation scheme for autoencoders, called *Simplex Interpolation*, in which we make the reconstructions corresponding to simplex interpolations of real latent samples look realistic. This is realized using an adversarial loss, where a discriminator is trained to predict simplex coefficients given the reconstructed images, and the autoencoder is trained to fool the discriminator (see Fig. 3). The proposed interpolation scheme yields a better-clustered latent representation.

The resulting autoencoder performs extremely well on the unsupervised anomaly detection task. On CIFAR-10 dataset, using a leave-one-out evaluation protocol, the best performing prior approach can only obtain a AUC score of around 0.74 (refer Table. 1). Our approach, on the other hand, achieves a substantial performance gain of 0.23 AUC points, thus achieving a new state-of-the-art for the problem. In particular, even for harder classes like *Bird*, in which prior approaches consistently under-perform, our approach achieves a performance gain over 50%. Our approach is versatile, and can be applied on non-image datasets as well. We achieve the state-of-the-art performance on three non-image datasets: KDD99, Thyroid and Arrhythmia, especially obtaining an improvement of over 50% on Thyroid dataset.

In summary, our key contributions are as follows:

- We propose a novel autoencoder model, called *Mirrored Adversarial Autoencoder*, in which we replace the L_p loss with an adversarial loss involving joint distribution of original image and the reconstructed one.

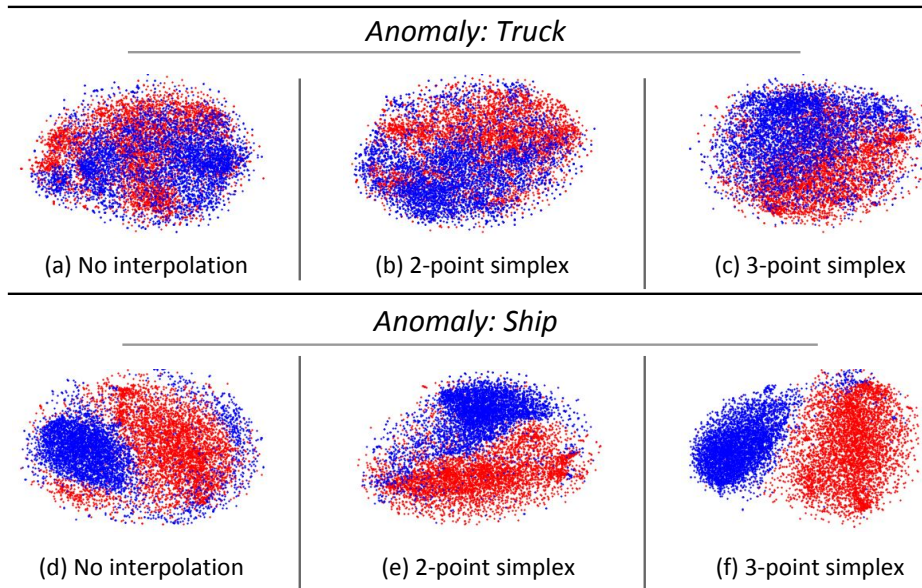


Fig. 2: T-SNE visualization of latent space using different interpolation techniques: Blue points denote anomalous samples, while red points denote normal samples. "No interpolation" denotes a mirrored autoencoder model trained with no interpolation. The panel on the top shows TSNE with *truck* class in CIFAR-10 dataset used as the anomaly class, while the panel on the bottom shows TSNE using *ship* as the anomaly class. All models are trained on the other 9 CIFAR-10 categories leaving out the anomaly class. We find that simplex interpolation results in good separation of latent space of normal and anomaly samples (More results are shown in supplementary material).

- We propose a novel interpolation scheme, called *Simplex adversarial interpolation* to obtain a rich clustered and semantically meaningful latent representation in an auto-encoder.
- The two schemes are used in the unsupervised anomaly detection problem, where we achieve the state-of-the-art results on CIFAR-10, KDD99, Thyroid and Arrhythmia datasets.

2 Related Work

Traditional methods for anomaly detection has been surveyed in detail in [7] [17] [33]. Some techniques for unsupervised anomaly detection includes using one-class SVM [24] to find the classification boundary of the normal data, using clustering method [25] to force similarity between members from the same cluster, etc. Eskin [8] project data points into feature space and find anomalous points in the sparsity region of feature space. However, these methods can only be used on low dimensional data distributions, perform poorly in high dimensional settings.

Recently, there has been much interest in using deep generative models for unsupervised anomaly detection. Approaches are either based on GAN, Au-

toEncoder or Variational Auto-Encoder model. Zhou [32] build a robust denoising auto encoder model, and detects anomalous samples using reconstruction error. Zong [34] and Zhai [31] directly learns a generative model on normal data distribution using mixture of Gaussians.

One of the first works that uses GAN model for anomaly detection is [23]. A GAN model is trained on normal samples, and a technique for inverting images to latent space is proposed. At test time, both normal samples and abnormal ones are mapped into the latent space and the generator model reconstructs them. Anomaly score is calculated using an L_2 norm between the difference of normal samples and the reconstructions. [1] [2] [5] train GAN model simultaneously with an encoder network for mapping images back into the latent space. Zenati [30] propose ALAD model, which is a BiGAN network for anomaly detection. FGAN [14] trains a GAN model to generate images along boundary of the normal distribution, and directly uses the discriminator score as anomaly threshold.

3 Interpolation

Interpolation is a way to enhance the structure of the latent space in an autoencoder. By forcing intermediate points along the interpolation to be indistinguishable from real data distribution, Berthelot *et al.* [6] find that the representation in latent space gets enhanced, leading to improved performance on downstream tasks such as supervised learning and clustering.

First, let us understand why interpolation can improve anomaly detection. Consider the Figure. 2(a) - the TSNE visualization of normal and anomalous latents of a vanilla autoencoder. Even though the autoencoder is trained only on normal samples, we find that the latent space of anomaly samples is mixed up with normal samples. This results in poor anomaly detection performance. Ideally, we would like to have a loss function that separates the manifolds of normal and anomaly samples. However, the absence of anomaly samples in the training phase prohibits using such a loss term. Instead, we can perform space filling, where we force the space between normal latents to be occupied by in-distribution samples. This will produce tight clustering of normal distributions, and anomaly distributions will inevitable fall out of this cluster. Simplex interpolation is an exact realization of this space filling. By forcing reconstructions of convex-hulls of normal samples look realistic, we fill the space between the latent distributions of normal samples.

3.1 Background: Berthelot et al.’s Interpolation

Berthelot *et al.* [6] investigates the use of adversarial loss to force the semantic consistency in image space using interpolation in latent space. First, latents corresponding to pairs of input images are generated, and a convex combination of the these latents are formed and decoded. A critic network takes this decoded image as input, and attempts to recover the coefficient of convex combination. The autoencoder is then trained so that the critic fails (assigns a coefficient 0).

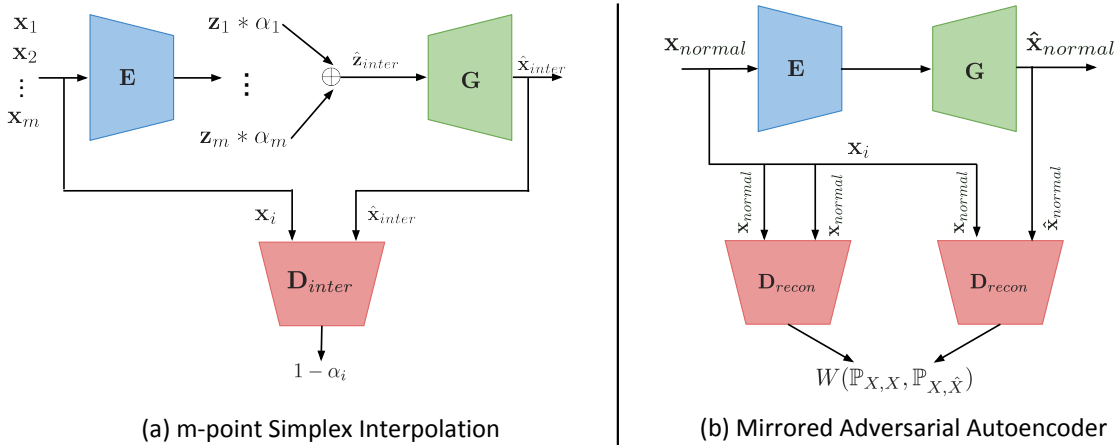


Fig. 3: **Frameworks.** On the left panel, we show m -point simplex interpolation. $\mathbf{D}_{\text{inter}}$ predicts how far the decoded interpolated image is from the original image, while autoencoder is trained to fool the discriminator. On the right panel, we show Mirrored Adversarial Autoencoder (MAE) model. MAE is trained to minimize the Wasserstein distance between the joint distribution of (input, input) and (input, reconstruction) samples.

Let us denote the encoder and decoder network as \mathbf{E} and \mathbf{G} respectively. For two data points \mathbf{x}_1 and \mathbf{x}_2 , $\mathbf{z}_1 = \mathbf{E}(\mathbf{x}_1)$ and $\mathbf{z}_2 = \mathbf{E}(\mathbf{x}_2)$ are their latent representations. Then, the linear interpolation of these two points can be represented as: $\hat{\mathbf{z}}_{\text{inter}} = \alpha \mathbf{z}_1 + (1 - \alpha) \mathbf{z}_2$, where α is constrained to be in the range $[0, 0.5]$. $\hat{\mathbf{z}}_{\text{inter}}$ is first decoded as $\mathbf{G}(\hat{\mathbf{z}}_{\text{inter}})$, which is then passed the critic network $\mathbf{D}_{\text{inter}}$. $\mathbf{D}_{\text{inter}}$ is trained to distinguish real samples from interpolated ones by predicting 0 for non-interpolated inputs, and α for interpolated samples. The loss that $\mathbf{D}_{\text{inter}}$ optimizes can be written as:

$$\min_{\mathbf{D}_{\text{inter}}} \|\mathbf{D}_{\text{inter}}(\mathbf{G}(\hat{\mathbf{z}}_{\text{inter}})) - \alpha\|^2 + \|\mathbf{D}_{\text{inter}}(\gamma \mathbf{x}_1 + (1 - \gamma) \hat{\mathbf{x}}_1)\|^2 \quad (1)$$

Meanwhile, autoencoder is trained to fool $\mathbf{D}_{\text{inter}}$ to give 0 for interpolations.

$$\min_{\mathbf{E}, \mathbf{G}} \|\mathbf{D}_{\text{inter}}(\mathbf{G}(\hat{\mathbf{z}}_{\text{inter}}))\|^2$$

3.2 Our proposal: m -point Simplex Interpolation

In this section, we introduce our simplex interpolation scheme. Our method includes a number of modifications to the Berthelot *et al.*'s [6] interpolation method. First, we train the $\mathbf{D}_{\text{inter}}$ on the joint distribution of the training images and the decoded interpolated images to force the encoder to generate semantically similar images from points close in latent space, rather than simply forcing all interpolated images to be indistinguishable from the training set as a whole, as in the Berthelot et al. formulation. Secondly, we extend line interpolation to

simplex interpolation to cover more points in the latent space. This results in improved space-filling.

Two-point Simplex Interpolation. In order to estimate the distance of image generated from interpolated point to two non-interpolated images, we introduce a discriminator $\mathbf{D}_{\text{inter}}$ trained on joint distribution of real and decoded interpolated image. For a given pair of training images, an interpolated image is first generated by decoding a convex combination of their latents. $\mathbf{D}_{\text{inter}}$ is trained separately on pairs of each of the image and the interpolating point to recover the distance in latent space between the encodings of each of the two training images and the interpolated image. The formula can be formalized as:

$$\begin{aligned} \hat{\mathbf{z}} &= \alpha \mathbf{E}(\mathbf{x}_1) + (1 - \alpha) \mathbf{E}(\mathbf{x}_2) \\ \hat{\mathbf{x}}_{\text{inter}} &= \mathbf{G}(\hat{\mathbf{z}}) \end{aligned} \quad (2)$$

$$\min_{\mathbf{D}_{\text{inter}}} \|\mathbf{D}_{\text{inter}}(\mathbf{x}_1, \hat{\mathbf{x}}_{\text{inter}}) - (1 - \alpha)\|^2 + \|\mathbf{D}_{\text{inter}}(\mathbf{x}_2, \hat{\mathbf{x}}_{\text{inter}}) - \alpha\|^2$$

$\mathbf{D}_{\text{inter}}$ always gives 0 to the pair of points that share the same semantics. When α equals 1, $\mathbf{D}_{\text{inter}}(\mathbf{x}_1, \hat{\mathbf{x}}_{\text{inter}})$ should give us 0 since $\hat{\mathbf{x}}_{\text{inter}} = \mathbf{G}(\mathbf{E}(\mathbf{x}_1))$ and it should have same semantic meaning as x_1 . On the other hand, $\mathbf{D}_{\text{inter}}(\mathbf{x}_2, \hat{\mathbf{x}}_{\text{inter}})$ is supposed to output 1 since $\hat{\mathbf{x}}$ and \mathbf{x}_2 have totally different semantic meanings.

A general case. Sainburget al. [21] argue that pairwise interpolation between samples of \mathbf{x} do not reach all points within the latent distribution, and will not necessarily make the latent distribution convex. Simplex Interpolation can cover points that line interpolation cannot cover. However, the loss function defined in Berthelot *et al.* [6] algorithm (Eq. (1)) is tailored for 2-point interpolation, and replacing Eq. (1) for predicting α vector instead of the scalar coefficient did not converge. Our approach (Eq.(2)), on the other hand, can be directly extended for m - point simplex interpolation since it measures how far interpolant is from each vertex of the simplex. The equations can be written as:

$$\begin{aligned} \hat{\mathbf{z}} &= \alpha_1 \mathbf{E}(\mathbf{x}_1) + \alpha_2 \mathbf{E}(\mathbf{x}_2) + \alpha_3 \mathbf{E}(\mathbf{x}_3) \quad s.t. \alpha_1 + \alpha_2 + \alpha_3 = 1 \\ \hat{\mathbf{x}}_{\text{inter}} &= \mathbf{G}(\hat{\mathbf{z}}) \end{aligned} \quad (3)$$

$$\min_{\mathbf{D}_{\text{inter}}} \sum_{i=1}^3 \|\mathbf{D}_{\text{inter}}(\mathbf{x}_i, \hat{\mathbf{x}}_{\text{inter}}) - (1 - \alpha_i)\|^2$$

Meanwhile, the autoencoder is trained to fool $\mathbf{D}_{\text{inter}}$ to give 0 for interpolated points, which can be written as

$$\min_{\mathbf{G}, \mathbf{E}} \sum_{i=1}^n \alpha_i \|\mathbf{D}_{\text{inter}}(\mathbf{x}_i, \hat{\mathbf{x}}_{\text{inter}})\|^2$$

where n is the number of images used to interpolate ($n = 2$ corresponds to 2-point simplex interpolation). Note that in Berthelot *et al.*'s formulation [6] there is no α_i term before the $\mathbf{D}_{\text{inter}}$ since they just consider the distance of decoded interpolated image to one of original images. However, in our algorithm, α_i is very crucial for the following reason: If $\alpha_k > \alpha_i$, then decoded image $\hat{\mathbf{x}}_{\text{inter}}$ is

Model	Bird	Car	Cat	Deer	Dog	Frog	Horse	Plane	Ship	Truck	Avg.
Fence GAN [14]	0.67	0.71	0.68	0.75	0.66	0.79	0.75	0.51	0.52	0.73	0.68
EGBAD [30]	0.38	0.51	0.44	0.37	0.48	0.35	0.52	0.57	0.41	0.56	0.46
Ano-GAN [23]	0.41	0.49	0.39	0.33	0.39	0.32	0.39	0.52	0.57	0.51	0.43
Skip-GANomaly [2]	0.44	0.95	0.60	0.69	0.61	0.93	0.78	0.80	0.66	0.91	0.73
2-point Interpolation	0.89	0.93	0.98	0.97	0.83	0.96	0.97	0.99	0.99	0.92	0.94
3-point Interpolation	0.910	0.969	0.93	0.99	0.90	0.99	0.973	0.99	0.99	0.970	0.961

Table 1: Anomaly detection performance on CIFAR-10 dataset. Each column denotes an anomaly class. Performance is reported in AUC scores.

closer to \mathbf{x}_k . Hence, the encoder-decoder loss corresponding to \mathbf{x}_k should receive a higher weight. Similarly, if α_k equals 0, $\hat{\mathbf{x}}_{inter}$ has no relation to \mathbf{x}_k , therefore there is no need to force \mathbf{G} and \mathbf{E} to generate a $\hat{\mathbf{x}}_{inter}$ close to \mathbf{x}_k . So, we propose scaling the discriminator loss with the α term.

4 Mirrored Adversarial AutoEncoder

For any autoencoder training, either L_1 or L_2 reconstruction loss between original image and its reconstruction has been used, which can be define as $\|\mathbf{x} - \mathbf{x}_{rec}\|_p$ where $p = 1, 2$. We propose to replace the pixel-level losses with a semantic-level reconstruction loss that is suited for the unsupervised anomaly detection.

L_1 or L_2 reconstruction losses typically result in blurry reconstructions. Moreover, using it as an anomaly score provides poor estimates as L_p distances do not measure the semantic similarity between images. Additionally, a high L_p reconstruction loss between input and decoded image can be an outcome of poor reconstruction quality and not because the image is an outlier, hence it results in poor anomaly scores. Our proposal is to replace L_p reconstruction loss with a novel adversarial loss, which is motivated by the following reasons: (1) To improve the quality of reconstructions, (2) Use of discriminator to obtain a semantically meaningful measure of anomaly score.

4.1 Reconstruction Discriminator \mathbf{D}_{recon}

We use a discriminator \mathbf{D}_{recon} to measure the Wasserstein distance between the joint distribution (\mathbf{x}, \mathbf{x}) and $(\mathbf{x}, \hat{\mathbf{x}})$. This approach differs from conventional Wasserstein GAN-based architectures [3] as joint distribution between image and reconstructed images are minimized instead of the marginal distributions. The reason for using such a discriminator is as follows: For training autoencoders, we are required to reconstruct a sample that looks similar to that of input sample. Just minimizing the Wasserstein distance between marginals of real and generated samples might result in a situation where input and generated sample both belong to the same distribution, yet semantically different. For example, a cat image in a CIFAR dataset can be reconstructed as an airplane. This will still be a feasible solution since both airplane and cat belong to the same input distribution, hence wasserstein distance will be small.

To resolve this issue, we perform Wasserstein minimization between the joint distributions $\mathbb{P}_{X,X}$ and $\mathbb{P}_{X,\hat{X}}$. The discriminator now takes in pairs of input images (\mathbf{x}, \mathbf{x}) and $(\mathbf{x}, \hat{\mathbf{x}})$. This clearly avoids the problems discussed in the previous section as the distribution (\mathbf{x}, \mathbf{x}) always has pairs of samples that are similar looking. If a car image reconstructs as airplane, the generated distribution will contain (car, airplane) sample, which is never found in the input distribution (\mathbf{x}, \mathbf{x}) . Hence, the model will always generate samples sharing the same semantics. We would like to point out that the formulation presented here is equivalent to matching conditional distributions between $W(\mathbb{P}_{X|X}, \mathbb{P}_{\hat{X}|X})$. This model also shares similarities to discriminator architectures used in conditional image to image translation such as Pix2Pix [10].

Mathematically, our formulation can be written as:

$$W(\mathbb{P}_{X,X}, \mathbb{P}_{X,\hat{X}}) = \max_{\mathbf{D}_{\text{recon}} \in \text{Lip-1}} \mathbb{E}_{x \sim X} [\mathbf{D}_{\text{recon}}(\mathbf{x}, \mathbf{x}) - \mathbf{D}_{\text{recon}}(\mathbf{x}, \hat{\mathbf{x}})] \quad (4)$$

where $\hat{\mathbf{x}} = \mathbf{G}(\mathbf{E}(\mathbf{x}))$

Lemma 1. *If E and G are optimal encoder and generator networks, i.e., $\mathbb{P}_{X,\mathbf{G}(\mathbf{E}(X))} = \mathbb{P}_{X,X}$, then $\mathbf{x} = \mathbf{G}(\mathbf{E}(\mathbf{x}))$*

4.2 Latent Space Regularizer

In addition to Wasserstein minimization between joint distributions of image-reconstruction pairs, we use a latent space regularization to regularize the norm of the latent codes. We find this regularization useful in practice for obtaining good anomaly detection scores.

$$R(\mathbf{E}) := \mathbb{E}_{\mathbf{x} \sim \mathbb{P}_X} \left[\max \left(\left\| \mathbf{E}(\mathbf{x}) - \sqrt{d} \right\|_2, 0 \right) \right]$$

where d is the dimension size of your latent space representation.

5 Unsupervised Anomaly Detection

The previous sections discussed two techniques for training autoencoders with improved latent representations: *Simplex Interpolation* and *Mirrored Adversarial Autoencoders*. In this section, we discuss how such autoencoder models can be used for unsupervised anomaly detection problem. The use of simplex interpolation helps obtain a compact and a clustered latent space for normal samples. As discussed in Section. 3, interpolation performs space-filling where the space between latent distributions of normal samples are made to look like normal distribution. Hence, latent codes of anomaly samples has to lie outside this distribution, which naturally gives a good separation between normal and anomaly regions in the latent space. This results in improved anomaly detection performance. *Mirrored Adversarial Autoencoders*, as discussed in Section. 4, learns autoencoders using an adversarial loss based on Wasserstein minimization between joint distributions of real and decoded samples. The learnt discriminator



Fig. 4: **Autoencoder reconstructions:** The panel on the left shows input and reconstructions of samples from normal distribution, while panel on the right shows it on anomaly distribution. In each panel, the top row corresponds to input and the bottom row shows reconstructions. While the quality of reconstructions are good for normal samples, anomaly samples are either reconstructed as birds or blurry images.

network provides a good feature representation to detect if the tuple of (input, reconstruction) sample belongs to the input distribution. We show that this discriminator representation provides a good estimate of anomaly score.

5.1 Training objective

First, we would like to point out that two discriminator models are used in our training pipeline: $\mathbf{D}_{\text{inter}}$ - discriminator used in interpolation step of *simplex adversarial interpolation*, and $\mathbf{D}_{\text{recon}}$ - discriminator used in reconstruction step in autoencoder training. $\mathbf{D}_{\text{inter}}$ and $\mathbf{D}_{\text{recon}}$ are updated according to Eq. (3) and Eq. (4) respectively. Encoder-decoder pair, on the other hand, has the following two objectives: (1) Autoencoder update: Minimizing the Wasserstein distance between the joint distribution of (X, X) and (X, \hat{X}) , and (2) Interpolation update: Forcing the interpolated points to look realistic. Overall objective can be written as:

$$\begin{aligned}
 & \max_{\mathbf{D}_{\text{recon}} \in \text{Lip}-1} \mathbb{E}_{x \sim X} [\mathbf{D}_{\text{recon}}(\mathbf{x}, \mathbf{x}) - \mathbf{D}_{\text{recon}}(\mathbf{x}, \hat{\mathbf{x}})] \\
 & \min_{\mathbf{D}_{\text{inter}}} \sum_{i=1}^3 \|\mathbf{D}_{\text{inter}}(\mathbf{x}_i, \hat{\mathbf{x}}_{\text{inter}}) - (1 - \alpha_i)\|^2 \\
 & \min_{\mathbf{G}, \mathbf{E}} \mathbb{E}_{\mathbf{x} \sim \mathbb{P}_X} \left[\lambda \left(\sum_{i=1}^n \alpha_i \|\mathbf{D}_{\text{inter}}(\mathbf{x}_i, \hat{\mathbf{x}}_{\text{inter}})\|^2 \right) \right] \\
 & \quad + \mathbb{E}_{\mathbf{x} \sim \mathbb{P}_X} [-\mathbf{D}_{\text{recon}}(\mathbf{x}, \mathbf{G}(\mathbf{E}(\mathbf{x}))) + R(\mathbf{E})]
 \end{aligned} \tag{5}$$

where λ is a scalar hyper-parameter which controls the weight of the interpolation loss. n denotes the number of images used to interpolate ($n = 2$ corresponds to 2-point interpolation).

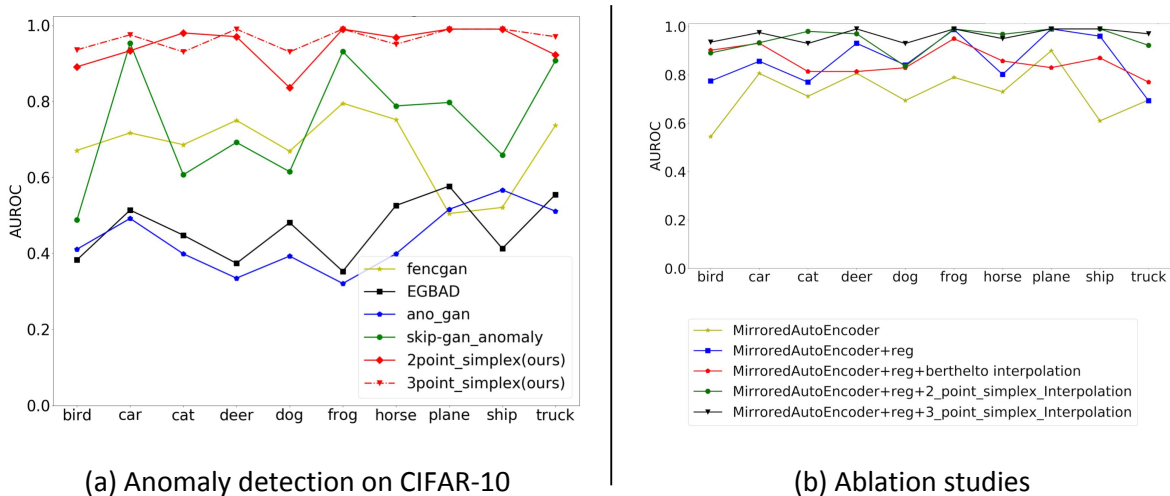


Fig. 5: In the left panel, we show anomaly detection AUC scores on CIFAR-10 dataset. Our approach significantly improves AUC scores over prior approaches on all settings. On the right panel, we show some ablation studies on use of regularizers and of varying m in m -point simplex interpolation.

5.2 Anomaly Score

Let $f(\mathbf{x}, \mathbf{y})$ denote the response of the pen-ultimate layer of the discriminator network $\mathbf{D}_{\text{recon}}$ when the pair (\mathbf{x}, \mathbf{y}) is used as input. This gives the feature embedding of the pair of points (\mathbf{x}, \mathbf{y}) . We define anomaly score as the L_1 norm difference between the feature embeddings:

$$L_{\text{rec_loss}} = \|f(\mathbf{x}, \mathbf{x}) - f(\mathbf{x}, \mathbf{G}(\mathbf{E}(\mathbf{x})))\|_1$$

Similar measures of anomaly scores are used by [2, 30].

6 Experiments

CIFAR10. To test unsupervised anomaly detection on CIFAR-10 dataset, we used the commonly-used leave-one-out protocol [1] [2], in which a sample from one of the CIFAR-10 classes is used as an anomalous sample, and all other 9 classes are used as normal samples (training data). Since the setting is unsupervised, training data only consists of normal data and anomalous samples should not be used while training. Experiments are repeated for 10 trials, each time using one of the CIFAR-10 classes as anomaly.

Our approach is optimized using the objective function 5. For the exact algorithm, please refer to the Supplementary material. In all our models, we used $\lambda = 0.5$. To optimize \mathbf{G} , $\mathbf{D}_{\text{inter}}$ and $\mathbf{D}_{\text{recon}}$ models, we used Adam optimizer with initial learning rate = $3e-4$, and momentum $\beta_1 = 0$, $\beta_2 = 0.999$. The encoder model \mathbf{E} is optimized using Adam optimizer with initial learning rate = $3e-4$ and momentum $\beta_1 = 0.5$, $\beta_2 = 0.999$. Among all models trained, we pick the best

Dataset	Model	Precision	Recall	F1 score
KDD99	IF [13]	0.9216	0.9373	0.9294
	DSEBM-r [31]	0.8521	0.6472	0.7328
	DSEBM-e [31]	0.8619	0.6446	0.7399
	DAGMM [32]	0.9297	0.9442	0.9369
	AnoGAN [23]	0.8786	0.8297	0.8865
	ALAD [30]	0.9427	0.9577	0.9501
	3- Simplex (Ours)	0.9527	0.9677	0.9601
Arrhythmia	IF	0.5147	0.5469	0.5303
	DSEBM-r	0.1515	0.1513	0.1510
	DSEBM-e	0.4667	0.4565	0.4601
	DAGMM	0.4909	0.5078	0.4983
	AnoGAN	0.4118	0.4375	0.4242
	ALAD	0.5000	0.5313	0.5152
	3- Simplex (Ours)	0.5294	0.5625	0.5455
Thyroid	PAE-GMM	0.4532	0.4881	0.4688
	DSEBM-r	0.0404	0.0403	0.0403
	DSEBM-e	0.1319	0.1319	0.1319
	DAGMM	0.4766	0.4834	0.4782
	ALAD	0.4583	0.4681	0.4632
		3- Simplex (Ours)	0.6875	0.7021

Table 2: Anomaly detection performance on non-image tabular datasets. Our approach consistently improves the performance on all three datasets: KDD99, Arrhythmia and Thyroid.

Outlier	Fence GAN [14]	EGBAD [30]	Ano-GAN [23]	GANomaly [1]	Ours
0	0.900	0.780	0.620	0.800	0.991
1	0.910	0.300	0.492	0.300	0.982
2	0.900	0.692	0.399	0.900	0.992
3	0.850	0.527	0.335	0.700	0.996
4	0.820	0.494	0.393	0.700	0.995
5	0.843	0.453	0.321	0.780	0.993
6	0.830	0.582	0.399	0.800	0.998
7	0.880	0.387	0.516	0.690	0.974
8	0.850	0.413	0.567	0.800	0.991
9	0.737	0.525	0.511	0.500	0.899
Avg	0.852	0.515	0.455	0.697	0.979

Table 3: Anomaly detection performance (AUC scores) on MNIST dataset. Each column denotes an anomaly class.

model as the one that gives least discriminator feature difference loss (L_1 loss between the discriminator features of the input samples and the reconstructed ones) on training samples after 60 epochs. Experiments are performed using two NVIDIA GTX-2080TI GPUS.

To evaluate our models, we compute the anomaly scores for normal and anomalous samples, and measure their AUC scores. Plot of our AUC scores compared with other approaches are reported in Figure. 5. We find that our approach significantly improves the AUC scores compared to the prior approaches. On an average, we get an **improvement of ~ 0.25 AUC points**, which is a significant improvement. Additionally, most of the prior approaches fail (achieve a AUC score of less than 0.5) on hard classes like bird (In CIFAR-10, bird class is similar to airplane class). Our approach achieves a performance of $0.9AUC+$, which is a phenomenal improvement in performance in such hard classes.

Method	Config1		Config2		Config3	
	AUC score	F1 score	AUC score	F1 score	AUC score	F1 score
REAPER [11]	0.900	0.892	0.877	0.703	0.824	0.541
Outlier Pursuit [28]	0.908	0.902	0.837	0.686	0.822	0.528
DPCP [27]	0.900	0.882	0.859	0.684	0.804	0.511
L_1 thresholding [26]	0.991	0.978	0.992	0.941	0.991	0.897
R-graph [29]	0.997	0.990	0.996	0.970	0.996	0.955
GPND [16]	0.968	0.979	0.945	0.960	0.919	0.941
Ours	0.987	0.993	0.971	0.983	0.977	0.986

Table 4: Performance of our methods on Coil-100 dataset. *Config 1* - Inliers: One category of images, Outliers: 50%, *Config 2* - Inliers: Four category of images, Outliers: 25%, *Config 3* - Seven category of images, Outliers: 15%

Date	ALOCC DR [20]	ALOCC D [20]	DCAE [22]	GPND [16]	OCGAN [15]	Ours
FMNIST	0.88	0.82	0.899	0.932	0.977	0.994

Table 5: Mean One-class novelty detection on FMNIST dataset

MNIST. We also evaluate our simplex interpolation model on MNIST dataset. We used the same leave-one-out protocol as CIFAR10 experiment, data points from a class as anomalous sample and data points from the other 9 classes as normal samples. Training data only consists of normal data and anomalous samples should not be used while training. Experiments are repeated for 10 trials, each time using one of the MNIST classes as anomaly. The results on table 3 shows that our method can reach AUC around 0.97 in MNIST. Please refer to supplementary material for more details on model architectures and hyper-parameters.

Coil-100 and FMNIST. GPND [16] and OCGAN [15] also evaluate their performance on Coil-100 and FMNIST. We use the same experiment design to test our model performance on these two dataset. We take randomly n categories, where $n \in 1, 4, 7$ and randomly sample the rest of the categories for outliers. We repeat this procedure 30 times. Result in Table 4 shows our method can compete them in Coil-100.

For FMNIST, 80% of in-class samples are used for training, 20% of in-class samples are used for testing. Negative samples are randomly selected so that they take up 50% of the test dataset. We leave one class as normal and others as anomalous samples, the final AUC score is calculated as average of 10 labels. In Table 5, our method is able to compete OCGAN [15] on FMNIST dataset.

Experiments on non-image dataset. Our approach is versatile, and can be applied to non-image datasets as well. We evaluate our simplex interpolation model on publicly available tabular data set KDDCup99 10%, Arrhythmia and Thyroid [12]. In these datasets, 20% samples of KDDCup99, 15% of Arrhythmia, 2.5% of Thyroid are labelled as anomalous. We evaluate anomaly detection performance using Precision, Recall and F1 score metrics, as done in previous approaches [30, 31, 34]. We randomly sample 50% of the data as training set, and remove anomalous samples from these. The resulting dataset is used as our training data.

At test time, we assume that fraction of anomaly samples in each dataset is known (20% in KDDCup99, 15% in Arrhythmia, 2.5% in Thyroid). This is the protocol used in [30,31,34]. For the test set, we compute anomaly scores for each sample, sort them by anomaly scores and assign top- k % of samples as anomalous, where k is the percentage of anomaly samples in each dataset. With these are assignments as predictions, we compute the evaluation metrics. Results are reported in Table. 2. We observe that our approach achieves the state-of-the-art performance on all three datasets. In particular, we obtain **significant gains of ~ 0.25 performance points** on Thyroid dataset. Please refer to supplementary material for more details on model architectures and hyper-parameters.

Ablation study

Our objective function consists of three main components, as shown in Eq. (5): (1) Autoencoder training loss, (2) Simplex interpolation and (3) Latent space regularization. In this experiment, we perform an ablation study of each of these components. For all experiments, we use Mirrored Autoencoder as our base architecture. Among simplex interpolation, we compare against 2-point and 3-point interpolation. In our experiments, we observe that performance saturates beyond $n = 3$. Results of the ablation study for CIFAR-10 is provided in Fig. 5. We make following observations: (1) Interpolation improves performance compared to not using any interpolation, and (2) Among the different interpolation techniques, Simplex interpolation outperforms Berthello interpolation, (3) 3-point simplex interpolation achieves improvements over using 2-point interpolation. These best performance is obtained by using 3-point simplex interpolation with a combination of all three terms in the objective of Eq. (5)

7 Conclusion

In this paper, we introduced a new method for the unsupervised anomaly detection problem based on a novel representation learning technique using deep autoencoders that contains two novel components: (1) *Mirrored Adversarial Autoencoder* that replaces the L_p reconstruction loss in the autoencoder optimization objective with a novel adversarial loss to enforce semantic-level reconstruction, and (2) *Simplex Interpolation* that extends the interpolation idea of [6] to improve the structure of the latent space representation in the autoencoder. We showed that our proposed method improves the state-of-the-art by a large margin on benchmark anomaly detection datasets. We note that ideas proposed in this work can be potentially used in the semi-supervised anomaly detection problem where we have access to few anomaly samples during the training. We leave this for the future work.

8 Acknowledgment

This work was supported in part by NSF CAREER AWARD 1942230, a sponsorship from Capital One and IBM Faculty award.

References

1. Akçay, S., Abarghouei, A.A., Breckon, T.P.: Ganomaly: Semi-supervised anomaly detection via adversarial training. CoRR **abs/1805.06725** (2018), <http://arxiv.org/abs/1805.06725>
2. Akçay, S., Abarghouei, A.A., Breckon, T.P.: Skip-ganomaly: Skip connected and adversarially trained encoder-decoder anomaly detection. CoRR **abs/1901.08954** (2019), <http://arxiv.org/abs/1901.08954>
3. Arjovsky, M., Chintala, S., Bottou, L.: Wasserstein generative adversarial networks. In: Proceedings of the 34th International Conference on Machine Learning. Proceedings of Machine Learning Research, vol. 70, pp. 214–223. PMLR, International Convention Centre, Sydney, Australia (06–11 Aug 2017)
4. Balaaji, Y., Hassani, H., Chellappa, R., Feizi, S.: Entropic GANs meet VAEs: A statistical approach to compute sample likelihoods in GANs. In: Proceedings of the 36th International Conference on Machine Learning. Proceedings of Machine Learning Research, vol. 97, pp. 414–423. PMLR, Long Beach, California, USA (09–15 Jun 2019)
5. Berg, A., Ahlberg, J., Felsberg, M.: Unsupervised learning of anomaly detection from contaminated image data using simultaneous encoder training. CoRR **abs/1905.11034** (2019), <http://arxiv.org/abs/1905.11034>
6. Berthelot, D., Raffel, C., Roy, A., Goodfellow, I.J.: Understanding and improving interpolation in autoencoders via an adversarial regularizer. CoRR **abs/1807.07543** (2018), <http://arxiv.org/abs/1807.07543>
7. Chandola, V., Banerjee, A., Kumar, V.: Anomaly detection: A survey (2007)
8. Eskin, E., Arnold, A., Prerau, M., Portnoy, L., Stolfo, S.: A geometric framework for unsupervised anomaly detection: Detecting intrusions in unlabeled data. Applications of Data Mining in Computer Security **6** (02 2002). <https://doi.org/10.1007/978-1-4615-0953-0-4>
9. Hendrycks, D., Mazeika, M., Dietterich, T.: Deep anomaly detection with outlier exposure. In: International Conference on Learning Representations (2019), <https://openreview.net/forum?id=HyxCxhRcY7>
10. Isola, P., Zhu, J.Y., Zhou, T., Efros, A.A.: Image-to-image translation with conditional adversarial networks. CVPR (2017)
11. Lerman, G., McCoy, M.B., Tropp, J.A., Zhang, T.: Robust computation of linear models, or how to find a needle in a haystack. CoRR **abs/1202.4044** (2012), <http://arxiv.org/abs/1202.4044>
12. Lichman, M.: Uci machine learning repository. Online (2013), Available:<http://archive.ics.uci.edu/ml>
13. Liu, F.T., Ting, K.M., Zhou, Z.H.: Isolation-based anomaly detection. ACM Trans. Knowl. Discov. Data **6**(1) (Mar 2012). <https://doi.org/10.1145/2133360.2133363>, <https://doi.org/10.1145/2133360.2133363>
14. Ngo, C.P., Winarto, A.A., Kou, C.K.L., Park, S., Akram, F., Lee, H.K.: Fence GAN: towards better anomaly detection. CoRR **abs/1904.01209** (2019), <http://arxiv.org/abs/1904.01209>
15. Perera, P., Nallapati, R., Xiang, B.: OCGAN: one-class novelty detection using gans with constrained latent representations. CoRR **abs/1903.08550** (2019), <http://arxiv.org/abs/1903.08550>
16. Pidhorskyi, S., Almohsen, R., Adjeroh, D.A., Doretto, G.: Generative probabilistic novelty detection with adversarial autoencoders. CoRR **abs/1807.02588** (2018), <http://arxiv.org/abs/1807.02588>

17. Pimentel, M.A.F., Clifton, D.A., Clifton, L., Tarassenko, L.: Review: A review of novelty detection. *Signal Process.* **99**, 215–249 (Jun 2014). <https://doi.org/10.1016/j.sigpro.2013.12.026>, <http://dx.doi.org/10.1016/j.sigpro.2013.12.026>
18. Porwal, U., Mukund, S.: Credit card fraud detection in e-commerce: An outlier detection approach. *CoRR* **abs/1811.02196** (2018), <http://arxiv.org/abs/1811.02196>
19. Rajpurkar, P., Irvin, J., Bagul, A., Ding, D.Y., Duan, T., Mehta, H., Yang, B., Zhu, K., Laird, D., Ball, R.L., Langlotz, C., Shpanskaya, K.S., Lungren, M.P., Ng, A.Y.: MURA dataset: Towards radiologist-level abnormality detection in musculoskeletal radiographs. *CoRR* **abs/1712.06957** (2017), <http://arxiv.org/abs/1712.06957>
20. Sabokrou, M., Khalooei, M., Fathy, M., Adeli, E.: Adversarially learned one-class classifier for novelty detection. *CoRR* **abs/1802.09088** (2018), <http://arxiv.org/abs/1802.09088>
21. Sainburg, T., Thielk, M., Theilman, B., Migliori, B., Gentner, T.: Generative adversarial interpolative autoencoding: adversarial training on latent space interpolations encourage convex latent distributions. *CoRR* **abs/1807.06650** (2018), <http://arxiv.org/abs/1807.06650>
22. Sakurada, M., Yairi, T.: Anomaly detection using autoencoders with nonlinear dimensionality reduction. pp. 4–11 (12 2014). <https://doi.org/10.1145/2689746.2689747>
23. Schlegl, T., Seeböck, P., Waldstein, S.M., Schmidt-Erfurth, U., Langs, G.: Unsupervised anomaly detection with generative adversarial networks to guide marker discovery. *CoRR* **abs/1703.05921** (2017), <http://arxiv.org/abs/1703.05921>
24. Schölkopf, B., Williamson, R., Smola, A., Shawe-Taylor, J., Platt, J.: Support vector method for novelty detection. In: *Proceedings of the 12th International Conference on Neural Information Processing Systems*. pp. 582–588. NIPS’99, MIT Press, Cambridge, MA, USA (1999), <http://dl.acm.org/citation.cfm?id=3009657.3009740>
25. Smith, R., Bivens, A., Embrechts, M., Palagiri, C., Szymanski, B.: Clustering approaches for anomaly based intrusion detection. *Proceedings of Intelligent Engineering Systems Through Artificial Neural Networks* pp. 579–584 (01 2002)
26. Soltanolkotabi, M., Candès, E.J.: A geometric analysis of subspace clustering with outliers. *CoRR* **abs/1112.4258** (2011), <http://arxiv.org/abs/1112.4258>
27. Tsakiris, M.C., Vidal, R.: Dual principal component pursuit. *CoRR* **abs/1510.04390** (2015), <http://arxiv.org/abs/1510.04390>
28. Xu, H., Caramanis, C., Sanghavi, S.: Robust PCA via outlier pursuit. *CoRR* **abs/1010.4237** (2010), <http://arxiv.org/abs/1010.4237>
29. You, C., Robinson, D.P., Vidal, R.: Provable self-representation based outlier detection in a union of subspaces. *CoRR* **abs/1704.03925** (2017), <http://arxiv.org/abs/1704.03925>
30. Zenati, H., Romain, M., Foo, C.S., Lecouat, B., Chandrasekhar, V.R.: Adversarially learned anomaly detection. *CoRR* **abs/1812.02288** (2018), <http://arxiv.org/abs/1812.02288>
31. Zhai, S., Cheng, Y., Lu, W., Zhang, Z.: Deep structured energy based models for anomaly detection. *CoRR* **abs/1605.07717** (2016), <http://arxiv.org/abs/1605.07717>
32. Zhou, C., Paffenroth, R.C.: Anomaly detection with robust deep autoencoders. In: *Proceedings of the 23rd ACM SIGKDD International Conference on Knowledge Discovery and Data Mining*. pp. 665–674. KDD ’17, ACM, New York, NY, USA

- (2017). <https://doi.org/10.1145/3097983.3098052>, <http://doi.acm.org/10.1145/3097983.3098052>
33. Zimek, A., Schubert, E., Kriegel, H.P.: A survey on unsupervised outlier detection in high-dimensional numerical data. *Stat. Anal. Data Min.* **5**(5), 363–387 (Oct 2012). <https://doi.org/10.1002/sam.11161>, <http://dx.doi.org/10.1002/sam.11161>
 34. Zong, B., Song, Q., Min, M.R., Cheng, W., Lumezanu, C., ki Cho, D., Chen, H.: Deep autoencoding gaussian mixture model for unsupervised anomaly detection. In: *ICLR* (2018)

Supplementary Material

1 Training Algorithm

Training and Test Algorithm

Training Stage:

Required Hyperparameters:

Distribution of normal samples $\mathbb{P}_{normal_samples}$, Epoch
tfd (discriminator iterations per generator update),
Learning rate, λ , n(batch size)

Input: $\mathbf{x} \sim \mathbb{P}_{normal_samples}$

For i in 1:epoch:

For t in (1:tfd):

$\mathbf{D}_{interloss}$ = 3 -point simplex interpolation loss

$\mathbf{D}_{reconloss}$ = Eq.(4) in main paper

$\mathbf{D}_{totalloss}$ = $\mathbf{D}_{interloss}$ + $\mathbf{D}_{reconloss}$

$\mathbf{D}_{totalloss.backward}()$

Update \mathbf{D}_{inter} , \mathbf{D}_{recon}

EndFor

$$loss_1 = \frac{1}{n} \sum_{i=1}^n \left[\max \left(\left\| \mathbf{E}(\mathbf{x}_i) - \sqrt{d} \right\|_2, 0 \right) \right]$$

$$loss_2 = \frac{1}{n} \sum_{i=1}^n -\mathbf{D}_{recon}(\mathbf{x}_i, \mathbf{G}(\mathbf{E}(\mathbf{x}_i)))$$

$$loss_3 = \frac{1}{k} \sum_k \sum_{x_1 \dots x_j} \lambda \left(\sum_{i=1}^j \alpha_i \left\| \mathbf{D}_{inter}(\mathbf{x}_i, \hat{\mathbf{x}}_{inter}) \right\|^2 \right)$$

for k different $\{x_1 \dots x_j\}$ sets

$$loss = loss_1 + loss_2 + loss_3$$

$loss.backward()$

Update \mathbf{G} and \mathbf{E}

If epoch ≥ 60 :

$$loss_{feat} = \frac{1}{n} \sum_{i=1}^n \|f(\mathbf{x}_i, \mathbf{x}_i) - f(\mathbf{x}_i, \mathbf{G}(\mathbf{E}(\mathbf{x}_i)))\|_1$$

Pick best model based on smallest $loss_{feat}$

EndIf

EndFor

Testing Stage:

Input: $\mathbf{x} \sim \mathbb{P}_{test_samples}$

Anomaly_score (\mathbf{x}_i) = $\|f(\mathbf{x}_i, \mathbf{x}_i) - f(\mathbf{x}_i, \mathbf{G}(\mathbf{E}(\mathbf{x}_i)))\|_1$

2 Proof of Lemma 4.1

Lemma 1. *If E and G are optimal encoder and generator networks, i.e., $\mathbb{P}_{X, \mathbf{G}(\mathbf{E}(X))} = \mathbb{P}_{X, X}$, then $\mathbf{x} = \mathbf{G}(\mathbf{E}(\mathbf{x}))$*

Proof:

$$\begin{aligned} \mathbb{P}_{X, \hat{X}} &= \mathbb{P}_{X, X} \\ p(\hat{x} = k) &= \int_x p(x, \hat{x} = k) dx \\ &= p(x = k, \hat{x} = k) \end{aligned}$$

Therefore $p(\hat{x} = k)$ is meaningful only if when $\hat{x} = x$, which means $\mathbf{G}(\mathbf{E}(x)) = x$

3 Architecture

3.1 CIFAR10

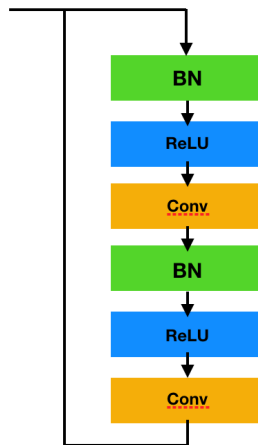


Fig. 1: ResBlock used in Generator and Discriminator: BN is replaced by Spectral Normal in \mathbf{D}_{recon} , BN is removed in \mathbf{D}_{inter}

Generator	Encoder	D_{recon}	D_{inter}
$z \in \mathbb{R}^{128}$	$x \in \mathbb{R}^{32 \times 32 \times 3}$	$(x, x) \in \mathbb{R}^{32 \times 32 \times 6}$	$(x, x) \in \mathbb{R}^{32 \times 32 \times 6}$
Dense, 4*4*256	((4,4),2,1,64)	ResBlock down 128	ResBlock down 128
ResBlock up 256	BN + leakylelu 0.2	ResBlock down 128	ResBlock down 128
ResBlock up 256	((4,4),2,1,128)	ResBlock 128	ResBlock 128
ResBlock up 256	BN + leakylelu 0.2	ResBlock 128	ResBlock 128
BN,ReLU,3 × 3 Conv,	((4,4),2,1,256)	ReLU	ReLU
Tanh	BN + leakylelu 0.2	Global sum pooling	Global average pooling
Adam($\beta_1=0, \beta_2=$	((4,4),1,0,128)	dense \rightarrow 1	dense \rightarrow 1
0.999)	Adam($\beta_1=0.5, \beta_2=$	Adam($\beta_1=0, \beta_2=$	Adam($\beta_1=0, \beta_2=$
	0.999)	0.999)	0.999)

LR = 3e-4, Batch Size = 256, Epoch=100, $\lambda = 0.5$

Table 1: We use architecture from Miyato [?] and Gulrajani [?], Encoder Structure is represented as (filter_size, stride, padding, output_channel)

3.2 MNIST

Generator	Encoder	D_{recon}	D_{inter}
$z \in \mathbb{R}^{64}$	$x \in \mathbb{R}^{28 \times 28 \times 3}$	$(x, x) \in \mathbb{R}^{28 \times 6}$	$(x, x) \in \mathbb{R}^{28 \times 28 \times 6}$
Linear(64,1024)+ReLU	Conv((4,4),2,2,64) +	Conv((4,4),2,2,64) +	Conv((4,4),2,2,64) +
Linear(1024,7*7*128)	leakylelu(0.2)	leakylelu(0.2)	leakylelu(0.2)
+ReLU	Conv((4,4),2,2,128) +	Conv((4,4),2,2,128) +	Conv((4,4),2,2,128) +
TransConv(4,4),2,2,64	leakylelu(0.2)	leakylelu(0.2)	leakylelu(0.2)
+ RELU	Dense(1024) +	Dense(1024) +	Dense(1024) +
TransConv(4,4),2,2,1 +	leakylelu(0.2)	leakylelu(0.2)	leakylelu(0.2)
Tanh	Dense(64)	Dense(1)	Dense(1)

LR = 1e-4, Batch Size = 256, Epoch=50, $\lambda = 0.5$, use same Adam parameters as CIFAR10

Table 2: MNIST Architecture Detail

3.3 KDD99

Generator	Encoder	D_{recon}	D_{inter}
$z \in \mathbb{R}^{32}$	$x \in \mathbb{R}^{121}$	$(x, x) \in \mathbb{R}^{121 \times 2}$	$(x, x) \in \mathbb{R}^{121 \times 2}$
Linear(32,64)+ReLU	Linear(121,64) +	Linear(242,128)	Linear(242,128)
Linear(64,128)+ReLU	leakylelu(0.2)	LeaklyRuLU(0.2)	LeaklyRuLU(0.2)
Linear(128,121)	Linear(64,32) +	Linear(128,25)	Linear(128,64)
Adam($\beta_1=0, \beta_2=0.5$)	leakylelu(0.2)	LeaklyRuLU(0.2)	LeaklyRuLU(0.2)
	Adam($\beta_1=0, \beta_2=0.5$)	Linear(25,1)	Linear(64,1)
		Adam($\beta_1=0, \beta_2=0.5$)	Adam($\beta_1=0, \beta_2=0.5$)

LR = 1e-4, Batch Size = 256, Epoch=50, $\lambda = 0.5$

Table 3: KDD99 Architecture Detail

3.4 Arrhythmia

Generator	Encode r	$\mathbf{D}_{\text{recon}}$	$\mathbf{D}_{\text{inter}}$
$\mathbf{z} \in \mathbb{R}^{64}$	$x \in \mathbb{R}^{274}$	$(x, x) \in \mathbb{R}^{274 \times 2}$	$(x, x) \in \mathbb{R}^{274 \times 2}$
Linear(64,128)+ReLU	Linear(274,256) +	Linear(274×2,256)	Linear(274×2,256)
Linear(128,256)+ReLU	leakylelu(0.2)	LeaklyRuLU(0.2)	LeaklyRuLU(0.2)
Linear(256,274)	Linear(256,128) +	Linear(256,32)	Linear(256,128)
Adam($\beta_1=0, \beta_2=0.5$)	leakylelu(0.2)	LeaklyRuLU(0.2)	LeaklyRuLU(0.2)
	Linear(128,64) +	Linear(32,1)	Linear(128,64)
	leakylelu(0.2)	Adam($\beta_1=0, \beta_2=0.5$)	LeaklyRuLU(0.2)
	Adam($\beta_1=0, \beta_2=0.5$)		Linear(64,1)
			Adam($\beta_1=0, \beta_2=0.5$)

LR = 2e-4, Batch Size = 32, Epoch=50, $\lambda = 0.3$

Table 4: Arrhythmia Architecture Detail

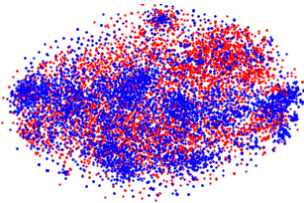
3.5 Thyroid

Generator	Encoder	$\mathbf{D}_{\text{recon}}$	$\mathbf{D}_{\text{inter}}$
$\mathbf{z} \in \mathbb{R}^4$	$x \in \mathbb{R}^6$	$(x, x) \in \mathbb{R}^{6 \times 2}$	$(x, x) \in \mathbb{R}^{274 \times 2}$
Linear(4,13)+ReLU	Linear(6,12)	Linear(6×2, 4)	Linear(6×2,6),
Linear(13,6)	leakylelu(0.2)	LeaklyRuLU(0.2)	ReLU(0.2)
SGD(momentum=0.5)	Linear(12,4)	Linear(4, 1)	Linear(6,1)
	leakylelu(0.2)	SGD(momentum=0.5)	SGD(momentum=0.5)
	SGD(momentum=0.5)		

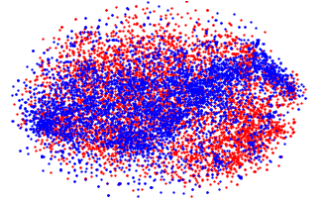
LR = 2e-5, Batch Size = 64, Epoch=100, $\lambda = 1.2$

Table 5: Thyroid Architecture Detail

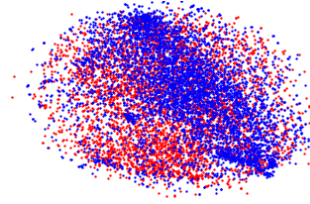
4 TSNE projection of latent space representation under different interpolation techniques



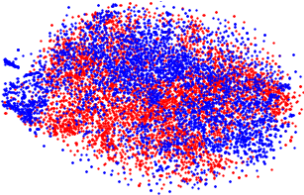
(a) Bird as anomaly class with no interpolation



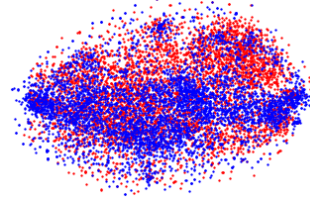
(b) Bird as anomaly class with 2-point simplex interpolation



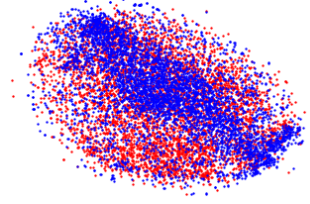
(c) Bird as anomaly class with 3-point simplex interpolate



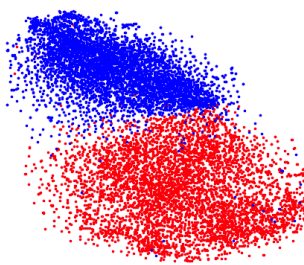
(a) Car as anomaly class with no interpolation



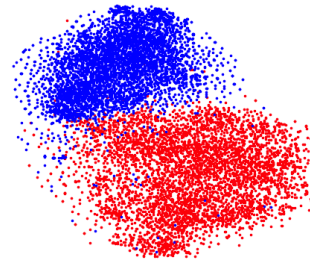
(b) Car as anomaly class with 2-point simplex interpolation



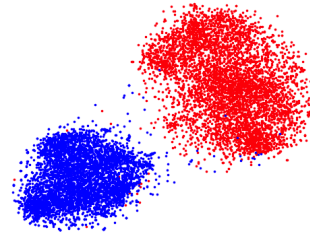
(c) Car as anomaly class with 3-point simplex interpolation



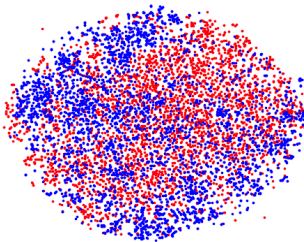
(a) Frog as anomaly class with no interpolation



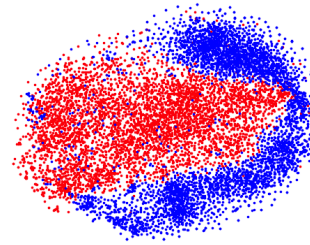
(b) Frog as anomaly class with 2-point simplex interpolation



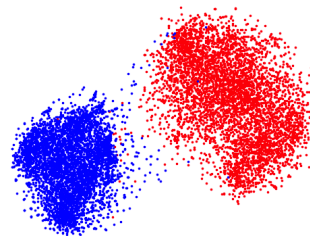
(c) Frog as anomaly class with 3-point simplex interpolation



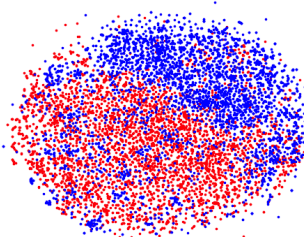
(a) Plane as anomaly class with no interpolation



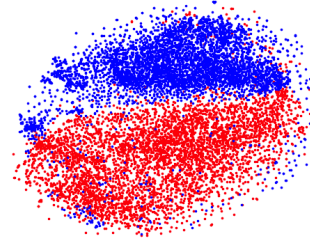
(b) Plane as anomaly class with 2-point simplex interpolation



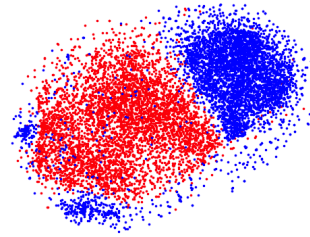
(c) Plane as anomaly class with 3-point simplex interpolation



(a) Deer as anomaly class with no interpolation



(b) Deer as anomaly class with 2-point simplex interpolation



(c) Deer as anomaly class with 3-point simplex interpolation